Heliyon 10 (2024) e29775

Contents lists available at ScienceDirect

Heliyon

journal homepage: www.cell.com/heliyon

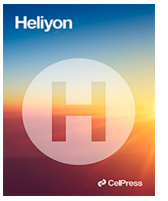

Research article

Deep learning assisted fluid volume calculation for assessing anti-vascular endothelial growth factor effect in diabetic macular edema

Yixiao Jin [a,b,1], Shuanghao Yong [c,1], Shi Ke [a,b], Chaoyang Zhang [a,b], Yan Liu [a,b], Jingyi Wang [a,b], Ting Lu [d], Yong Sun [d,**], Haiyan Wang [e,***], Jingfa Zhang [a,b,*]

[a] *Department of Ophthalmology, Shanghai General Hospital, Shanghai Jiao Tong University, School of Medicine, Shanghai, China*
[b] *National Clinical Research Center for Eye Diseases, Shanghai Clinical Research Center for Eye Diseases, Shanghai Key Clinical Specialty, Shanghai Key Laboratory of Ocular Fundus Diseases, Shanghai Engineering Center for Visual Science and Photomedicine, Shanghai Engineering Center for Precise Diagnosis and Treatment of Eye Diseases, Shanghai, China*
[c] *School of Electrical Engineering and Automation, Anhui University, Hefei, China*
[d] *Department of Ophthalmology, Jiading Branch of Shanghai General Hospital, Shanghai Jiao Tong University School of Medicine, Shanghai, China*
[e] *Department of Ocular Fundus, Shaanxi Eye Hospital, Xi'an People's Hospital (Xi'an Fourth Hospital), Xi'an, Shaanxi, China*

A B S T R A C T

Objective: To develop an algorithm using deep learning methods to calculate the volume of intraretinal and subretinal fluid in optical coherence tomography (OCT) images for assessing diabetic macular edema (DME) patients' condition changes.
Design: Cross-sectional study.
Participants: Treatment-naive patients diagnosed with DME recruited from April 2020 to November 2021.
Methods: The deep learning network, which was built for autonomous segmentation utilizing an encoder-decoder network based on the U-Net architecture, was used to calculate the volume of intraretinal fluid (IRF) and subretinal fluid (SRF). The alterations of retinal vessel density and thickness, and the correlation between best-corrected visual acuity (BCVA) and OCT parameters were analyzed.
Results: 2,955 OCT images of fourteen eyes from DME patients with IRF and SRF who received anti-vascular endothelial growth factor (VEGF) agents were obtained. The area under the curve (AUC) of the receiver operating characteristic (ROC) curve of the algorithm was 0.993 for IRF and 0.998 for SRF. The volumes of IRF and SRF were significantly decreased from 1.93 ± 0.58 /1.14 ± 0.25 mm^3 (baseline) to 0.26 ± 0.13 /0.26 ± 0.18 mm^3 (post-injection), respectively ($p = 0.0170$ for IRF, and $p = 0.0004$ for SRF). The Spearman correlation demonstrated that the reduction of IRF volume was negatively correlated with age (coefficient $= -0.698$, $p = 0.006$).
Conclusion: We developed a deep learning assisted fluid volume calculation algorithm with high sensitivity and specificity for assessing the volume of IRF and SRF in DME patients. **Key words**: deep learning; diabetic macular edema; optical coherence tomography.

* Corresponding author. Department of Ophthalmology, Shanghai General Hospital, Shanghai Jiao Tong University School of Medicine, 100 Hai Ning Road, Shanghai, 200080, China.
** Corresponding author. Department of Ophthalmology, Jiading Branch of Shanghai General Hospital, Shanghai Jiao Tong University School of Medicine, Shanghai, 201803, China.
*** Corresponding author. Shaanxi Eye Hospital, Xi'an People's Hospital (Xi'an Fourth Hospital), Xi'an, 710004, Shaanxi, China.
E-mail addresses: drsunyong@aliyun.com (Y. Sun), whyeye@126.com (H. Wang), 13917311571@139.com (J. Zhang).
[1] Yixiao Jin and Shuanghao Yong are co-first authors contributed equally to this study.

https://doi.org/10.1016/j.heliyon.2024.e29775
Received 20 September 2023; Received in revised form 14 April 2024; Accepted 15 April 2024
Available online 17 April 2024

1. Introduction

Diabetic macular edema (DME) can appear in any stage of diabetic retinopathy (DR), which occurs due to the deregulation of fluid entry and exit, with the accumulation of intraretinal fluid (IRF) and subretinal fluid (SRF) [1,2]. Currently, several randomized controlled trials have conclusively demonstrated that intravitreal injections of anti-vascular endothelial growth factor (VEGF) drugs, such as aflibercept and ranibizumab, can produce superior visual outcomes than conventional laser therapy [3].

Optical coherence tomography (OCT)/OCT-angiography (OCTA), which detect retinal lesions in multiple layers with segmentation in a non-invasive fashion, are widely used in clinic assessments of DME.

The majority of available OCT analysis software in clinical practice is restricted to measuring the layer thickness of the retina, such as the central macular thickness (CMT) [4,5], despite the fact that previous research has demonstrated the limited utility of this biomarker for visual prognosis and disease management [6]. However, CMT can vary significantly between individuals due to several variables, including age, sex, refractive status, etc. [7–9]. For example, women have thinner retinas than men, so it is more likely to be missed diagnosis of centrally involved edema in women [10]. Due to the overlap between normal populations and diabetic patients, there will theoretically always be a certain number of false positives and false negatives, regardless of the threshold used. In addition, other macular pathological characteristics, such as the preretinal membrane or DR-induced retinal atrophy, may increase or reduce CMT. Direct measurement of the changes in fluid volume, an intrinsic characteristic of DME, does not have the above limitations, which may be more sensitive and specific than thickness measurement.

Previous studies have developed several algorithms and demonstrated their efficacy in fluid volume detection. Nevertheless, these methods possess several drawbacks, including low precision in segmenting data [11], the need for human intervention [12], rigorous requirements for raw data [13] and the absence of manual annotations and effective constraints [14]. Therefore, a better optimal approach is needed to determine the fluid volume in OCT images. This study aims to develop an algorithm using deep learning to calculate the volume of IRF and SRF of DME patients to evaluate anti-VEGF therapy.

2. Materials and methods

2.1. Patients enrollment

This study enrolled 14 eyes from 12 treatment-naïve DME patients with both IRF and SRF at baseline. This study followed the Declaration of Helsinki's principles and was reviewed by the ethical committee of Shanghai General Hospital, affiliated with Shanghai Jiao Tong University (2023-263).

The inclusion criteria for this study were: ① diagnosis of type 1 or type 2 diabetes; ② the presence of SRF in the fovea with IRF (0–1 mm diameter from the central point of fovea) at the baseline. The exclusion criteria were: ① patients who didn't consent to participate in this study or did not cooperate with the examinations; ②patients with other ocular fundus diseases, such as age-related macular degeneration, retinal vein occlusion, or choroidal neovascularization, or with a history of intraocular surgery within 3 months; ③ low quality ophthalmic images (the detailed description of image quality was described in Supplementary Table 1).

All patients were intravitreally injected with anti-VEGF agents, including aflibercept (8 eyes) and conbercept (6 eyes). The intravitreal injection and follow-up procedure were described previously [15,16].

2.2. Parameters for evaluation

Data were collected, including age, sex, BCVA, volume of IRC and SRF, vessel density, and other OCT variables.

2.3. Image dataset

Macular scans of 6×6 mm^2 were obtained with OCT (Optovue Inc., Fremont, CA, USA) approximately one week after intravitreal injection in all patients. 2955 OCT images of B- scan from different layers were collected from 14 eyes.

2.4. Deep learning of automatic segmentation

In this study, the VGG16 (Visual Geometry Group) [17] deep convolutional neural network is selected as the backbone to determine the main parameters of the original U-net convolutional layers to encode the input images. The encoder of this study consists of five convolutional modules, from shallow to deep, which is responsible for extracting the features of original images. The decoder part, composed of four upsampling modules, is responsible for recombining and restoring the features. Every module consists of an upsampling layer and a convolutional layer that concatenate corresponding features from different depths to gradually reconstruct the encoding. The integrated flowchart of this deep learning method was presented in Supplementary Fig. 1.

The data pre-processing, training process, hardware, and software parameters are briefly described as follows: 159 labeled slice images were the training set, with 40 images as the validation set. To prevent overfitting, data augmentation was performed: ① resizing and distorting the input image, with a transformation threshold of 0.2–2 for the length and width; ② flipping the image horizontally. The batch size of the network was set to 2, and a total of 100 iterations of training were performed, with the first 50 iterations being frozen to improve training efficiency, and the remaining 50 iterations being unfrozen. The Adam optimizer was used as the optimization algorithm for the network, and the learning rate was dynamically adjusted based on the training situation.

Additionally, an independent external dataset [18] was employed to ensure an unbiased evaluation of this model. Among them, 50 images were enrolled as testing set.

The primary hardware environment for the experiments in this study was Intel Xeon® Silver 4114 CPU and Nvidia TESLA V100 32G GPU, and the deep learning framework used was PyTorch.

2.5. Volumetric calculation analysis

The volume of IRF, SRF and fluid in INL at each visit were calculated according to the Cavalieri principle of stereological analysis [19,20]. The volume calculation is limited to a 1 mm circle centered from the central fovea. First, the areas of macular fluid in individual OCT slices were quantified based on the aforementioned deep learning algorithm. Subsequently, the fluid volume between two contiguous slices was defined as the average area of two sequential slices multiplied by the fixed interval (0.015 mm between two adjacent slices in OCT AngioVue software). Finally, the summation of volume from every separating segment demonstrated the total volume in the retina. The unit for volume is mm^3.

2.6. Mixed-effects model analysis

Concerning binocular collinearity and mutual influence, the mixed-effects model was employed in data analysis. This model is particularly suitable for analyzing data with multiple layers or group structures, such as repeated measurements from the same subject. The fixed effects of interest were the change in edema volume pre- and post-treatment, and the individual differences of patients were considered random effects. The "readxl" and "lme4″ packages in R software were utilized.

2.7. Statistical analysis

R software (R Foundation for Statistical Computing, Vienna, Austria) and EmpowerStats version 2.0 (X&Y solutions Inc., Boston, MA, USA) were employed for all the statistical analyses. *P*-value <0.05 was interpreted as statistically significant and mean ± standard error of mean (SEM) was used to describe quantitative results.

3. Results

3.1. General clinical characteristics

Table 1 and Supplementary Table 2 summarized the characteristics of study participants. The average age of participants at baseline was 58.43 ± 2.91 years. At the initial visit, the mean BCVA was 0.54 ± 0.05 logMAR, while the BCVA improved to 0.42 ± 0.05 logMAR (p = 0.0058) at the final visit (Table 1).

Table 1
Demographic and clinical information of the participants.

Variable	Value (N = 14)	P value
Age, mean (SEM) [range], y	58.43 (2.91) [30–71]	
Sex, No.		
Male	4	
Female	8	
Eyes, No.		
OS	6	
OD	8	
Anti-VEGF agents, No.(eyes)		
Aflibercept	8	
Conbercept	6	
BCVA, mean (SEM) [range]		
Baseline	0.54 (0.05) [0.16–1.00]	0.0058
Post-injection	0.42 (0.05) [0.04–0.70]	
CMT, mean (SEM) [range], μm		
Baseline	532.70 (45.02) [340.00–874.00]	0.0004
Post-injection	284.70 (20.05) [200.00–453.00]	
IRF, mean (SEM) [range], mm^3		
Baseline	1.92 (0.58) [0.00–7.37]	0.0170
Post-injection	0.26 (0.13) [0.00–1.34]	
SRF, mean (SEM) [range], mm^3		
Baseline	1.14 (0.25) [0.25–3.29]	0.0004
Post-injection	0.26 (0.18) [0.00–2.35]	
Reduction of IRF, mean (SEM) [range], mm^3	1.66 (0.61) [-0.98-7.37]	
Reduction of SRF, mean (SEM) [range], mm^3	0.88 (0.19) [0.07–2.25]	

BCVA, best-corrected visual acuity; CMT, Central macular thickness; OD, oculus dexter, right eye; OS, oculus sinister, left eye; SEM, standard error of the mean.

3.2. Assessment of network performance

The elaborate structure of the classifier is illustrated in Fig. 1. The particular indices of this model (Table 2) and ROC curves (Fig. 2) were calculated. The promising specificity of the model for both IRF (0.996) and SRF (0.998) indicates that it achieves a high level of sensitivity and recognition for both types of cumulus (Table 2). Besides, the model has a higher recall value for SRF, suggesting that it can distinguish SRF regions more accurately than IRF (0.844 for SRF vs. 0.686 for IRF). Besides, the confusion matrix, intersection over union (IOU), pixel accuracy (PA), and mean pixel accuracy (MPA) were also calculated. The confusion matrices are as follows:

$$\begin{bmatrix} 5036813 & 18850 & 11327 \\ 27486 & 60087 & 0 \\ 13752 & 0 & 74565 \end{bmatrix}$$

Averaging the IOUs across categories gives mIOU = 0.7663. PA, which is the ratio of correctly predicted pixels to the total number of pixels, was calculated as 0.9864, and MPA, which is the average of the accuracies for each category, was calculated as 0.8415. The ROC curve showed that for the IRF and SRF, the AUC were 0.993 and 0.998 (Fig. 2A), and the precision-recall curve showed the AUC were 0.810 and 0.933 for IRF and SRF, respectively (Fig. 2B). Additionally, the performance of algorithm in external testing dataset was depicted in Supplementary Table 3 and representative segmentation images of external dataset were shown in Supplementary Fig. 2. The enrollment of external dataset, without data leakage and bias, ensured the reliability and robust classification ability.

3.3. Volumetric quantification of fluid volume

Intravitreal injection of anti-VEGF agent reduced the volume of IRF significantly (1.93 ± 0.58 mm^3 at baseline vs. 0.26 ± 0.13 mm^3 after injection, Fig. 3A), and the volume of SRF diminished significantly from 1.14 ± 0.25 mm^3 (baseline) to 0.26 ± 0.18 mm^3 (post-injection) (Fig. 3B). In addition, there was a significant reduction in the total volume of IRF and SRF after treatment (Fig. 3C). Similarly, in mixed-effects model, the fixed effects analysis indicated a significant difference in fluid volume before and after treatment, with an estimated difference of 1.6617 mm^3 for IRF ($t = 2.990$), and 0.8817 mm^3 for SRF ($t = 3.630$). Since the presence of disorganization within the inner nuclear layer (INL) has been identified as a predictor for visual acuity in DME [21] and the volume of fluid in INL has a strong correlation with visual acuity [22], the fluid volume within INL was also calculated. Consistently, the fluid volume in INL decreased significantly after treatment (Supplementary Fig. 3). Fig. 4 presents two representative examples. Patient 1

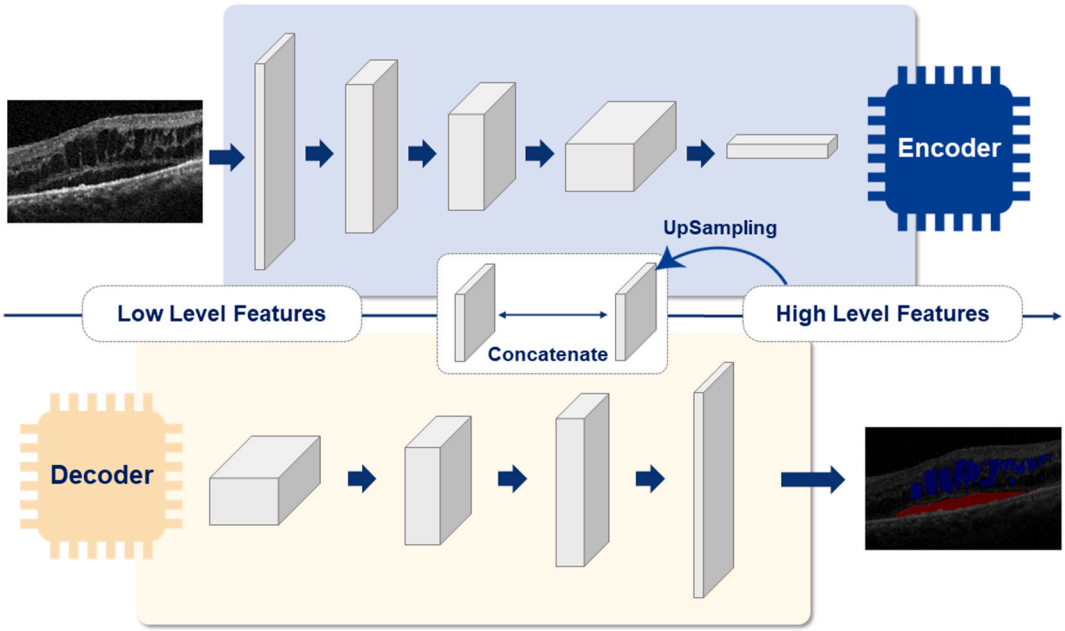

Fig. 1. The overall architecture of the encoder-decoder network.
The classifier is a complex function that computes the mapping relationship between the pixel values of an image and the pixel types. The classifier is trained and predicted on a single image basis, and the operational dimension of each image is the pixel dimension, which means that each pixel is classified (IRF, SRF, non-fluid). The gray bars in the schematic represent the extracted features. The classifier consists of encoders and decoders. The encoder extracts the deep features of the image, which are divided into 5 levels from shallow to deep. The decoder gradually restores the deep features back to the shallow features (the shallowest features are the picture itself), and the process of feature restoration at each level is spliced with the upper encoded features, with the purpose of computing the macroscopic connections between pixels and keeping the decoded dimensions consistent with the corresponding encoded levels. The final effect of decoding is to restore the same dimension as the original image, when the value of each pixel is the class predicted for the corresponding pixel of the original image.

Table 2
The performance of this deep learning assisted fluid volume calculation algorithm.

	Non-fluid	IRF	SRF
TP	5036813	60087	74565
FP	41238	18850	11327
TN	134652	5136457	5143236
FN	30177	27486	13752
Recall	0.994	0.686	0.844
Specificity	0.766	0.996	0.998
Precision	0.992	0.761	0.868
F1	0.993	0.722	0.856
ACC	0.986	0.991	0.995
AUC	0.992	0.993	0.998
IOU	0.986	0.565	0.748

TP: true positives; FP: false positives; TN: true negatives; FN: false negatives; ACC: accuracy; AUC: area under the curve; IOU: intersection over union; IRF: intraretinal fluid; SRF: subretinal fluid.

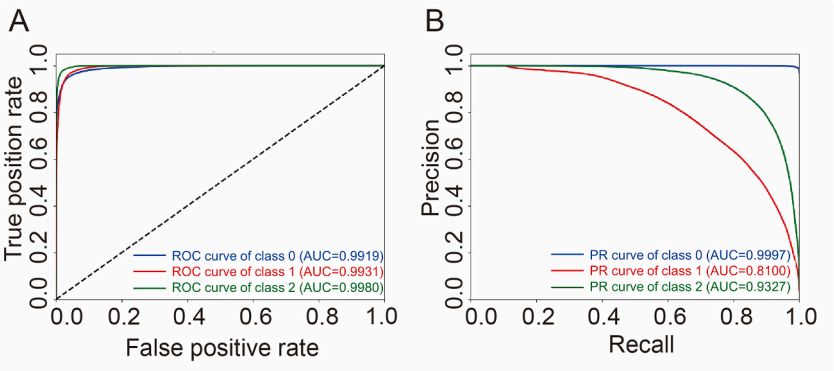

Fig. 2. Evaluation of the fluid segmentation results and receiver operating characteristic curves for test OCTA images. (A) The ROC curve; **(B)** the precision-recall curve. AUC, area under the curve; IRF, intraretinal fluid; ROC, receiver operating characteristic curve; SRF, subretinal fluid.

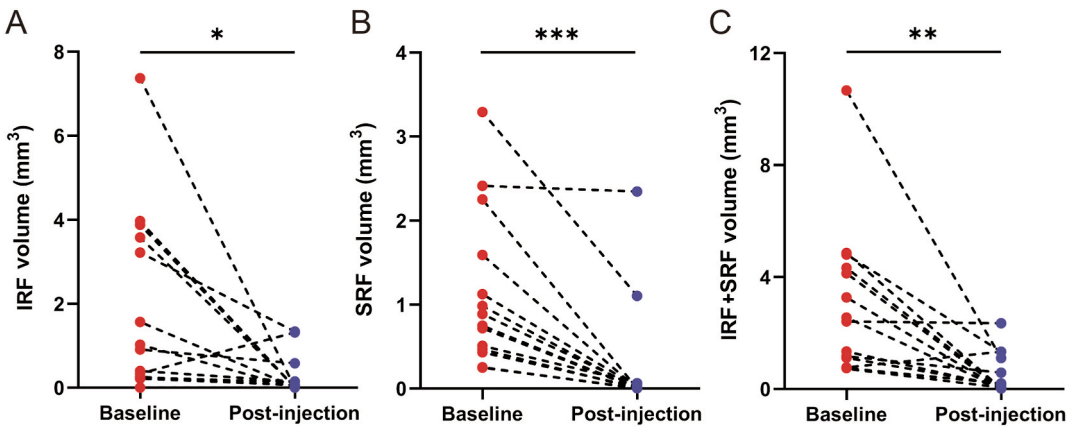

Fig. 3. Intravitreal injection of anti-VEGF agents was effective to decrease the volume of IRF and SRF. The reduction in IRF volume **(A)**, SRF volume **(B)**, and the total volume of IRF and SRF **(C)** were compared between the baseline and post-injection. *$p < 0.05$; **$p < 0.01$; ***$p < 0.001$; IRF, intraretinal fluid; SRF, subretinal fluid.

was a 50-year-old male with DME, IRF and SRF were observed at the 6 × 6 mm^2 sections centered on the fovea (Fig. 4A). The volume of IRF and SRF was reduced significantly, and the IRF almost disappeared (7.37 mm^3 and 3.29 mm^3 at baseline vs. 0.001 mm^3 and 1.10 mm^3 at final follow-up) after anti-VEGF treatment; Patient 2 was a 50-year-old man with DME (Fig. 4B). The volume of IRF and SRF reduced (3.58 mm^3 and 0.75 mm^3 at baseline vs. 0.04 mm^3 and 0 mm^3 at final follow-up), and the BCVA improved from logMAR 0.4 at baseline to logMAR 0.3 after treatment.

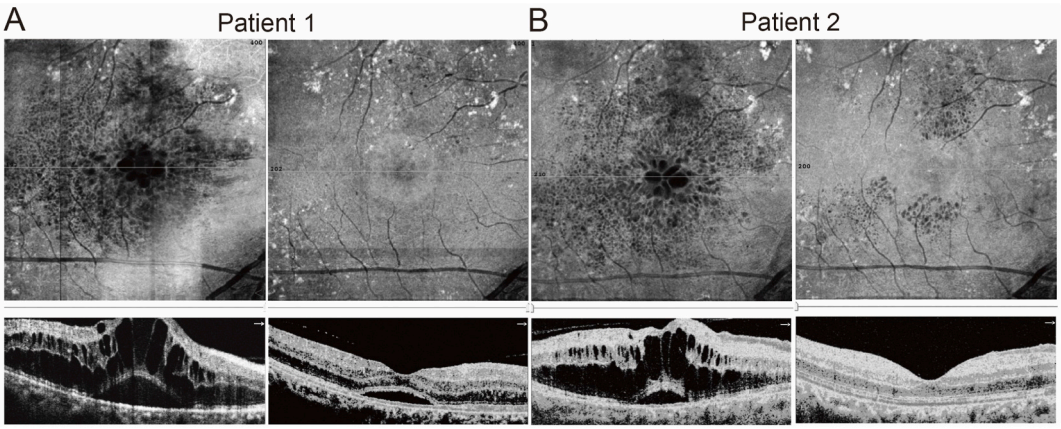

Fig. 4. Representative images of two patients demonstrating the IRF and SRF at baseline and after intravitreal anti-VEGF injections. (A) The OCTA image of patient 1 at baseline (left) and post-injection (right); **(B)** The OCTA image of patient 2 at baseline (left) and post-injection (right).

3.4. Correlation analysis with OCT parameters

The Spearman correlation revealed that the reduction of IRF volume was negatively correlated with age (coefficient = −0.698, p = 0.006, Fig. 5A), but not SRF (coefficient = −0.003, p = 0.992, Fig. 5B). In addition, the reduction of the total volume of IRF and SRF was also negatively correlated with age (coefficient = −0.700, p = 0.005, Fig. 5C). Correlation between BCVA and fluid volume in INL was also performed (Supplementary Fig. 4). In addition, correlations between CMT and other available OCTA characteristics were analyzed, and it was found that the association between CMT and SRF at baseline was statistically significant (Supplementary Table 4).

3.5. Alteration of retinal thickness and retinal vessel density after anti-VEGF treatment

Significant reductions in retinal thickness were observed in fovea (0–1 mm diameter from the central fovea) and para-fovea regions (1–3 mm diameter from central fovea), including the temporal, superior, nasal, and inferior of para-fovea (Fig. 6A). In contrast, no

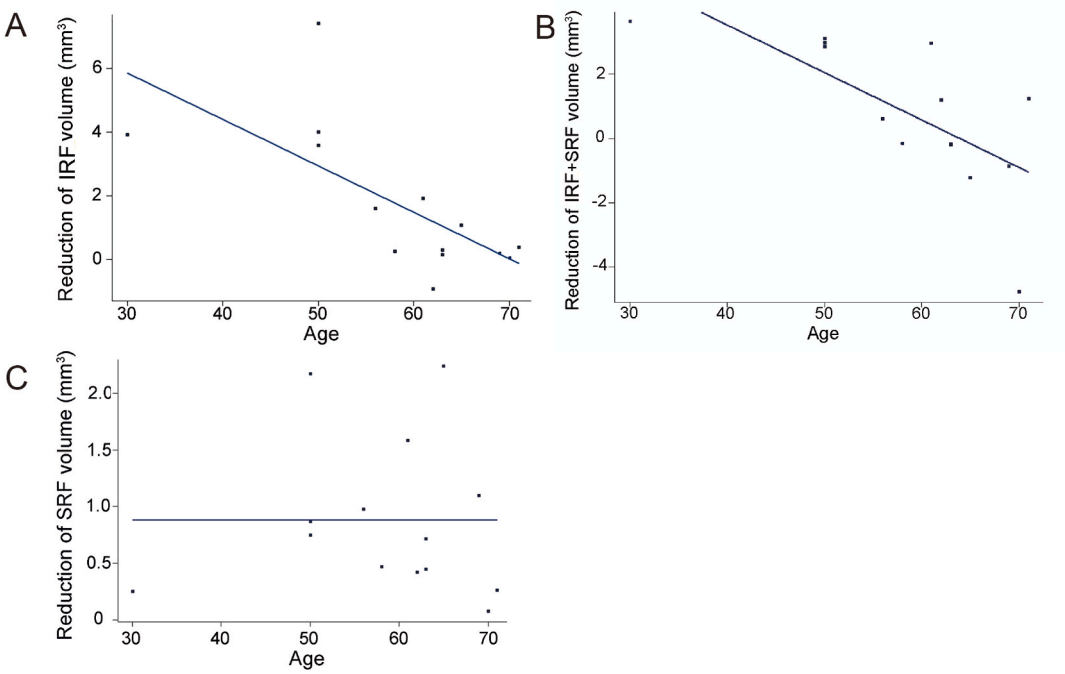

Fig. 5. Correlation analysis between age and OCTA characteristics. The correlations between age and reduction of IRF volume **(A)**, reduction of SRF volume **(B)**, and reduction of the total volume of IRF and SRF **(C)**. IRF, intraretinal fluid; SRF, subretinal fluid.

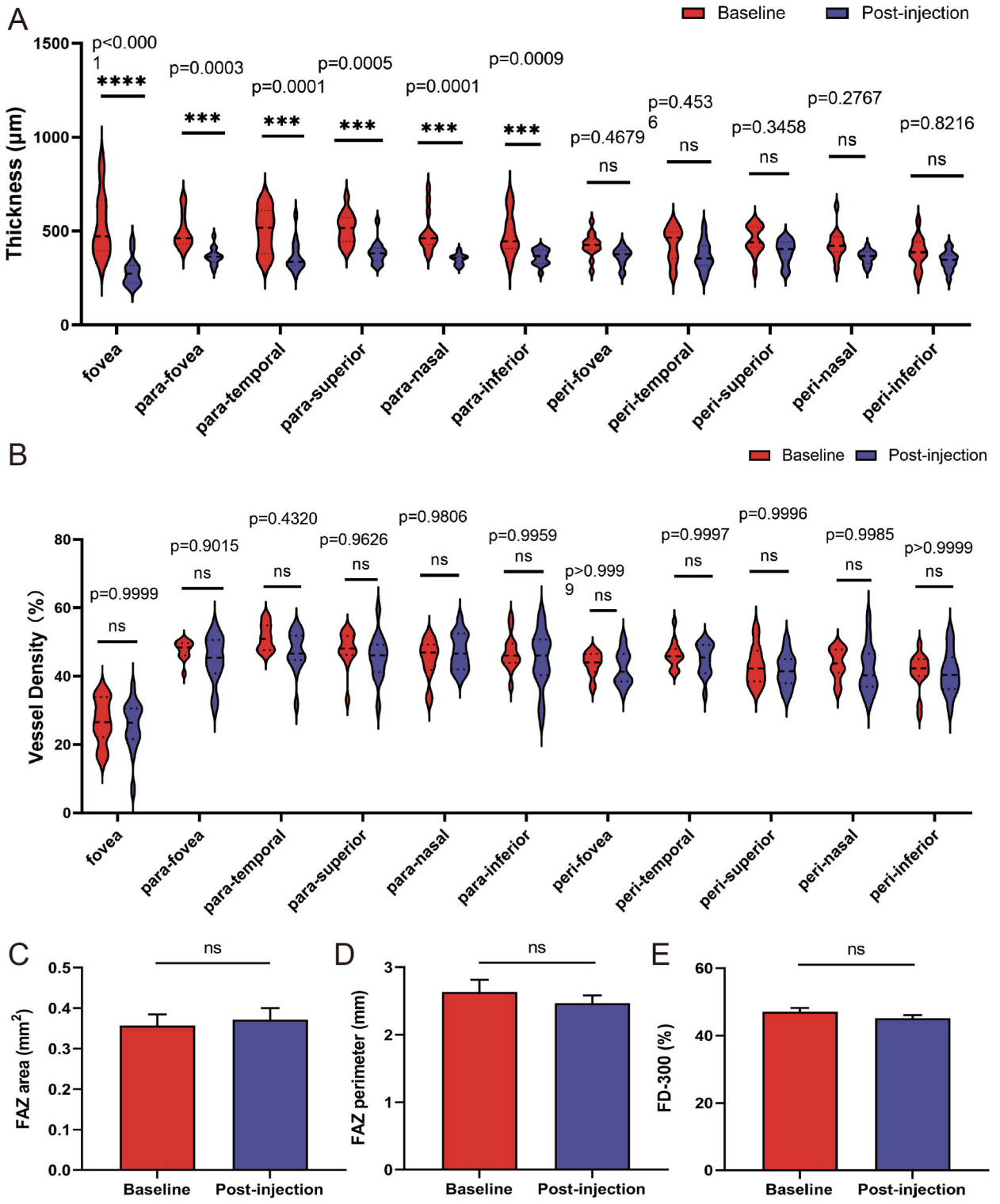

Fig. 6. Comparison of retinal thickness, vessel density, and other comparable parameters. Comparison of retinal thickness **(A)** and retinal vessel density **(B)** between the baseline and post-injection in different subareas of the macula. **(*C*–E)** Alterations of FAZ area **(C)**, FAZ perimeter **(D)**, and FD-300 **(E)** at the baseline and post-injection. FAZ, foveal avascular zone; FD-300, vessel density of foveal in a 300-μm wide annulus encircling the FAZ.

statistically significant changes were detected in any of the perifoveal regions (3–6 mm diameter from central fovea). There were no significant differences in vessel density between pre-injection and post-injection in all macular regions (Fig. 6B), as well as in the foveal avascular zone (FAZ) area (Fig. 6C), the FAZ perimeter (Fig. 6D), and the FD-300 (Fig. 6E).

4. Discussion

CMT has been widely used in clinical studies as a representative OCT parameter. However, CMT, as a two-dimensional parameter, could not fully reflect alterations of macular fluid in the three-dimensions [23]. In this study, we utilized 2955 OCT images and developed a deep learning-based algorithm to measure the volumetric change, which objectively interprets the efficacy of anti-VEGF therapy on the edema regression of DME patients. This model has high sensitivity and specificity for both IRF and SRF, and could discriminate the region of the fluid accurately. As SRF and IRF typically indicate the outer and inner blood-retinal barrier disruption, respectively, the differential accumulation patterns of IRF and SRF provide insights into the underlying pathophysiological mechanisms and may guide more targeted therapeutic interventions. Overall, these studies would facilitate physicians in determining disease activity and evaluating treatment effectiveness.

In this study, even though only 14 eyes were included, based on nearly 3000 OCT images at different layers, we still constructed a reliable algorithm for evaluating retinal fluid volume using deep learning, with multidimensional metrics assessment, including TP, FP, TN, FN, F1 score, AUC, IOU, PA, MPA, recall, precision, and specificity. It combines the feature extraction capability of the residual structure with the ability to coordinate global pixels of the U-net structure, demonstrating fast computation, high accuracy, and a broader range of applicability in experimental settings. Schlegl et al. proposed an encoder-decoder structure composed of convolutional and transpositional convolutional modules to accomplish semantic segmentation [11]. However, it could lose some critical feature information after multilayered convolutional modules with the linear network structure, which results in a lower upper limit of segmentation accuracy; Sometimes even experienced medical practitioners could find it difficult to reach consensus on ambiguous low-quality regions where the true segmentation type cannot be deduced from the image. De Fauw et al. employed multiple instances of the segmentation network to train and generate entire segmentation maps for a particular scan, which led to superior performance particularly in challenging scenarios with ambiguity and complexity [12]. In this study, the algorithm also performed well in low quality and blurred images by individually analyzing each pixel and predicting its classification according to confidence score, without any deliberate human intervention. Compared with existing relevant works, improvements in network architecture design and training methodology have rendered this model more advanced. Due to the relatively small scale of the available training dataset, a pre-trained weight scheme was introduced for transfer learning. Leveraging the universally applicable features extracted by the backbone network (VGG16 in this study) not only enhanced the performance on small dataset training but also accelerated the convergence rate. Simultaneously, it effectively mitigated overfitting issues, thereby endowing the model with superior generalization capabilities. Furthermore, in the process of training the neural network, freezing and thawing stages were devised, aiding in the better execution of retinal fluid classification tasks based on the pre-trained model. The incorporation of a dynamically adjusted learning rate balanced training efficiency and model performance.

In this study, the microvascular densities in the foveal, parafoveal, and perifoveal regions were detected and showed no change before and after treatment. In contrast to our results, previous studies have revealed that blood flow density decreases significantly following anti-VEGF therapy, especially patients who received more than 20 injections considerably reduced mean peripapillary flow index [24]. This phenomenon might likely be attributed to the inadequate duration provided for the regression of neovascularization over the follow-up period. Alterations in blood flow density over a short period are not sufficient to be detected by instruments (Fig. 6B), but the change of fluid volume could be observed (Fig. 3). This further implies that fluid volume, rather than vascular density, is the more sensitive indicator for determining the efficacy of anti-VEGF therapy. Similarly, Schmidt-Erfurth, Ursula et al. emphasized the potential of automated fluid quantification in enhancing therapeutic management and decision-making in neovascular age-related macular degeneration patients who received anti-VEGF therapy [25].

Consistent with previous findings [26–28], no significant correlation between BCVA and CMT as well as volume, was detected in the present study. Both volume and CMT have limited ability to determine BCVA because they predominantly evaluate edema and disregard many other aspects of DR, such as structural disorders and ischemia. Interestingly, a negative correlation between decrease in IRF volume and age was discovered, the same as the decrease in volume of IRF plus SRF. This indicated that anti-VEGF treatment was less effective for older patients. Although no statistically significant association has been observed between BCVA and fluid volume in INL, a trend does suggest that smaller fluid volume in INL tend to be associated with superior visual acuity, which is consistent with previous studies [22]. The limited number of patients may have contributed to the absence of statistically significant results, necessitating additional verification by the inclusion of a larger sample size.

This study has several limitations. First, as the high-resolution OCTA used in this study has denser scanning, which offers the possibility of accurate estimation of fluid volume, this deep learning-based algorithm may be limited in its applicability to more widely accessible structural OCT scans, which only equip a less-dense scan pattern. Second, this study did not determine the impact of clinical care and patients age [29] on therapeutic effects across patients, which could have influenced the findings. Third, in consideration of the limited sample size and relatively short observation period, there might be inherent biases that could potentially influence the generalizability. In future research, more patients, including those with resistance to anti-VEGF treatments or on other medications such as dexamethasone intravitreal implant, will be enrolled in the study to further validate the algorithm.

In conclusion, we developed a deep learning-assisted calculation algorithm with high sensitivity and specificity for assessing the volume of IRF and SRF in DME patients who received anti-VEGF treatment. Moreover, this methodology has the potential to facilitate ophthalmologists monitoring the condition change in OCT/OCTA images in patients with other ocular fundus diseases.

Ethics statement

This study was approved by the ethical committee of Shanghai General Hospital, affiliated with Shanghai Jiao Tong University (ethics approval number: 2023-263, and ethics approval date: July 20, 2023) in accordance with the Declaration of Helsinki. Written informed consent was obtained from all participants.

Consent to participate

Informed consent was obtained from all individual participants included in the study.

Funding

This work was supported by the National Natural Science Foundation of China (82171062, 82301222); the Joint Funds of the National Natural Science Foundation of China (U2267220); the Shanghai Science and Technology Innovation (20Y11910900); Shanghai Hospital Development Center (SHDC2020CR4081) and the Shanghai Key Clinical Specialty, Natural Science Foundation of Shanghai (20ZR1472600).

Data availability statement

Data will be made available on request.

CRediT authorship contribution statement

Yixiao Jin: Writing – review & editing, Writing – original draft, Visualization, Validation, Software, Methodology, Investigation, Formal analysis, Data curation, Conceptualization. **Shuanghao Yong:** Writing – original draft, Visualization, Software, Methodology, Formal analysis, Data curation. **Shi Ke:** Writing – original draft, Investigation, Formal analysis. **Chaoyang Zhang:** Validation, Investigation. **Yan Liu:** Validation, Investigation. **Jingyi Wang:** Validation, Investigation. **Ting Lu:** Validation, Investigation. **Yong Sun:** Writing – review & editing, Validation, Supervision, Project administration, Investigation. **Haiyan Wang:** Writing – review & editing, Validation, Supervision, Project administration, Investigation. **Jingfa Zhang:** Writing – review & editing, Validation, Supervision, Resources, Project administration, Investigation, Funding acquisition, Formal analysis, Data curation, Conceptualization.

Declaration of competing interest

The authors declare that they have no known competing financial interests or personal relationships that could have appeared to influence the work reported in this paper.

Appendix A. Supplementary data

Supplementary data to this article can be found online at https://doi.org/10.1016/j.heliyon.2024.e29775.

References

[1] A. Daruich, A. Matet, A. Moulin, et al., Mechanisms of macular edema: beyond the surface, Prog. Retin. Eye Res. 63 (2018) 20–68.
[2] J. Zhang, J. Zhang, C. Zhang, et al., Diabetic macular edema: current understanding, molecular mechanisms and therapeutic implications, Cells 11 (2022).
[3] G.S. Tan, N. Cheung, R. Simó, G.C. Cheung, T.Y. Wong, Diabetic macular oedema, Lancet Diabetes Endocrinol. 5 (2017) 143–155.
[4] N.M. Bressler, I. Odia, M. Maguire, et al., Association between change in visual acuity and change in central subfield thickness during treatment of diabetic macular edema in participants randomized to aflibercept, bevacizumab, or ranibizumab: a post hoc analysis of the protocol T randomized clinical trial, JAMA Ophthalmol 137 (2019) 977–985.
[5] N.M. Bressler, W.T. Beaulieu, M.G. Maguire, et al., Early response to anti-vascular endothelial growth factor and two-year outcomes among eyes with diabetic macular edema in protocol T, Am. J. Ophthalmol. 195 (2018) 93–100.
[6] U. Schmidt-Erfurth, S.M. Waldstein, A paradigm shift in imaging biomarkers in neovascular age-related macular degeneration, Prog. Retin. Eye Res. 50 (2016) 1–24.
[7] T. von Hanno, A.C. Lade, E.B. Mathiesen, T. Peto, I. Njølstad, G. Bertelsen, Macular thickness in healthy eyes of adults (N = 4508) and relation to sex, age and refraction: the Tromsø Eye Study (2007-2008), Acta Ophthalmol. 95 (2017) 262–269.
[8] W.K. Song, S.C. Lee, E.S. Lee, C.Y. Kim, S.S. Kim, Macular thickness variations with sex, age, and axial length in healthy subjects: a spectral domain-optical coherence tomography study, Invest. Ophthalmol. Vis. Sci. 51 (2010) 3913–3918.
[9] X.R. Duan, Y.B. Liang, D.S. Friedman, et al., Normal macular thickness measurements using optical coherence tomography in healthy eyes of adult Chinese persons: the Handan Eye Study, Ophthalmology 117 (2010) 1585–1594.
[10] K.V. Chalam, S.B. Bressler, A.R. Edwards, et al., Retinal thickness in people with diabetes and minimal or no diabetic retinopathy: heidelberg Spectralis optical coherence tomography, Invest. Ophthalmol. Vis. Sci. 53 (2012) 8154–8161.
[11] T. Schlegl, S.M. Waldstein, H. Bogunovic, et al., Fully automated detection and quantification of macular fluid in OCT using deep learning, Ophthalmology 125 (2018) 549–558.

[12] J. De Fauw, J.R. Ledsam, B. Romera-Paredes, et al., Clinically applicable deep learning for diagnosis and referral in retinal disease, Nat Med 24 (2018) 1342–1350.
[13] M.X. Li, S.Q. Yu, W. Zhang, et al., Segmentation of retinal fluid based on deep learning: application of three-dimensional fully convolutional neural networks in optical coherence tomography images, Int. J. Ophthalmol. 12 (2019) 1012–1020.
[14] K. Gao, S. Niu, Z. Ji, et al., Double-branched and area-constraint fully convolutional networks for automated serous retinal detachment segmentation in SD-OCT images, Comput Methods Programs Biomed 176 (2019) 69–80.
[15] J. Wu, C. Zhang, Q. Yang, et al., Imaging hyperreflective foci as an inflammatory biomarker after anti-VEGF treatment in neovascular age-related macular degeneration patients with optical coherence tomography angiography, BioMed Res. Int. 2021 (2021) 6648191.
[16] S. Qin, C. Zhang, H. Qin, et al., Hyperreflective foci and subretinal fluid are potential imaging biomarkers to evaluate anti-VEGF effect in diabetic macular edema, Front. Physiol. 12 (2021) 791442.
[17] K. Simonyan, A. Zisserman, Very deep convolutional networks for large-scale image recognition, CoRR (2014) 1556, abs/1409.
[18] D.S. Kermany, K. Zhang, M.H. Goldbaum, Large Dataset of Labeled Optical Coherence Tomography (OCT) and Chest X-Ray Images, 2018.
[19] Y.S. Prakash, K.G. Smithson, G.C. Sieck, Application of the Cavalieri principle in volume estimation using laser confocal microscopy, Neuroimage 1 (1994) 325–333.
[20] C. Balaratnasingam, L.A. Yannuzzi, C.A. Curcio, et al., Associations between retinal pigment epithelium and drusen volume changes during the lifecycle of large drusenoid pigment epithelial detachments, Invest. Ophthalmol. Vis. Sci. 57 (2016) 5479–5489.
[21] J.K. Sun, M.M. Lin, J. Lammer, et al., Disorganization of the retinal inner layers as a predictor of visual acuity in eyes with center-involved diabetic macular edema, JAMA Ophthalmol 132 (2014) 1309–1316.
[22] K. Tsuboi, Q.S. You, Y. Guo, et al., Association between fluid volume in inner nuclear layer and visual acuity in diabetic macular edema, Am. J. Ophthalmol. 237 (2022) 164–172.
[23] B.S. Gerendas, S. Prager, G. Deak, et al., Predictive imaging biomarkers relevant for functional and anatomical outcomes during ranibizumab therapy of diabetic macular oedema, Br. J. Ophthalmol. 102 (2018) 195–203.
[24] C. Türksever, L. Hoffmann, K. Hatz, Peripapillary and macular microvasculature in neovascular age-related macular degeneration in long-term and recently started anti-VEGF therapy versus healthy controls, Front. Med. 9 (2022) 1080052.
[25] U. Schmidt-Erfurth, W.D. Vogl, L.M. Jampol, H. Bogunović, Application of automated quantification of fluid volumes to anti-VEGF therapy of neovascular age-related macular degeneration, Ophthalmology 127 (2020) 1211–1219.
[26] Q.S. You, K. Tsuboi, Y. Guo, et al., Comparison of central macular fluid volume with central subfield thickness in patients with diabetic macular edema using optical coherence tomography angiography, JAMA Ophthalmol 139 (2021) 734–741.
[27] N. Liao, H. Jiang, G. Mao, et al., Changes in macular ultrastructural morphology in unilateral anisometropic amblyopia, Am J Transl Res 11 (2019) 5086–5095.
[28] Q. Wei, Z. Wan, Y. Hu, Q. Peng, Cytokine and chemokine profile changes in patients after intravitreal conbercept injection for diabetic macular edema, Drug Des Devel Ther 13 (2019) 4367–4374.
[29] S. Kusuhara, M. Shimura, S. Kitano, et al., Treatment of diabetic macular edema in real-world clinical practice: the effect of aging, J Diabetes Investig 13 (2022) 1339–1346.